Real-space ion scattering maps of the Mg(0001) surface

Robert D. Kolasinski,* Josh A. Whaley, and Robert Bastasz
Hydrogen and Metallurgical Science Department, Sandia National Laboratories, Livermore, California 94551, USA
(Received 13 March 2008; revised manuscript received 3 January 2009; published 9 February 2009)

Low-energy ion scattering (LEIS) is useful for examining the structure of ordered surfaces as well as for identifying surface atoms. However, in some cases the structural information from LEIS measurements is obscured by complex collision processes which contribute to the detected scattering intensity. In this study, we have developed a more precise approach for examining surface structure that includes comparing experimental real-space ion scattering maps with simulations from binary collision codes using reliability factors. This method is demonstrated with the model system 2 keV $Ne^+ \rightarrow Mg(0001)$. Using an angle-resolved ion energy spectrometer, the intensity of scattered Ne^+ from the surface was recorded for a complete set of polar and azimuthal angles, which define the orientation of the surface with respect to the incident beam. These angles were then transformed to distances in real space and used to compile an ion scattering map of the Mg(0001) surface. A simulated map was also generated for the same conditions using a modified version of the binary collision code MARLOWE. The maps provide a comprehensive overview of surface scattering and allow the locations of surface atoms to be correlated directly to regions of enhanced scattering intensity. The sensitivity of the LEIS signal to interatomic spacing was simulated using MARLOWE, and methods for comparing with experiments were developed. Because LEIS can distinguish different types of atoms on the surface, the techniques described here could be extended to map compound surfaces and adsorbates.

DOI: 10.1103/PhysRevB.79.075416 PACS number(s): 68.49.Sf, 34.50.−s

I. INTRODUCTION

Low-energy ion scattering (LEIS) provides information about the composition and structure of atoms on surfaces. For an analysis of surface composition, ions that undergo elastic binary collisions are of interest because the observed energy is related to the mass of the surface atom by classical kinematics. The local atomic structure, on the other hand, is revealed by considering the angular distribution of scattered ions. The feasibility of using LEIS for these applications was demonstrated in an early work by Smith,[1] and LEIS structure analysis was further developed, both in theory and experiment, by Williams and Yarmoff.[2]

Most previously published LEIS studies have obtained structural information by systematically varying the polar (α) or azimuthal (φ) angles of the incident beam with respect to the sample surface and monitoring the intensity of scattered ions at a fixed observation angle (θ).[3] (See Fig. 1 for definitions.) Such polar or azimuthal scans typically show variations in the intensity of scattered ions that are related to shadowing effects caused by neighboring atoms. A beam of incident ions deflected by surface atoms generates "shadow cones," which are regions of space in the vicinity of surface atoms that incident ions cannot reach. A diagram showing an axial cut through a shadow cone appears in Fig. 2. Note that the shadowed area is approximately parabolic in shape. An important characteristic is the accumulation of many trajectories at the shadow cone edge, and as a result, there is a sharp change in particle flux in moving across this boundary.

Shadow cone analysis allows for a straightforward interpretation of scattering intensity variations observed in LEIS. This approach has been used heavily in many previous LEIS structural studies; a review of the existing techniques is provided in Ref. 4. However, in many cases more complex scattering events occur on the surface which cannot be adequately described by shadowing alone, suggesting the need for more detailed methods. One such approach is real-space scattering maps. If the shadow cone shape is known, the angle of incidence, α, may be related to an intersection dis-

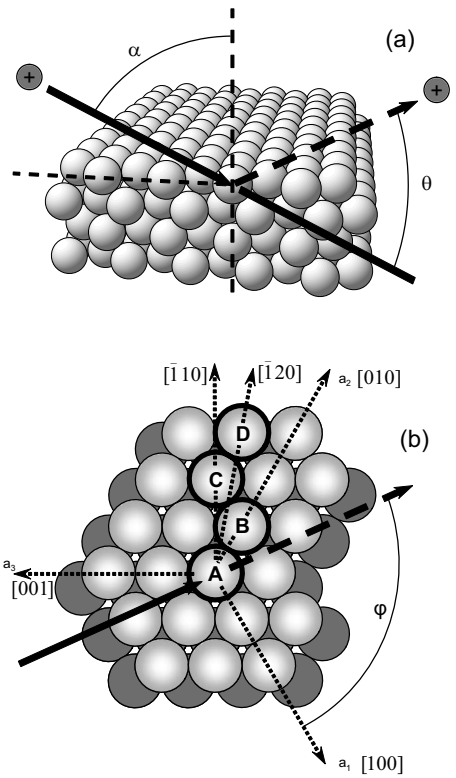

FIG. 1. (a) Side and (b) top views of the Mg(0001) surface showing angle definitions and reference axes. The first, second, and fourth nearest neighbors to atom A are indicated by atoms B, C, and D.

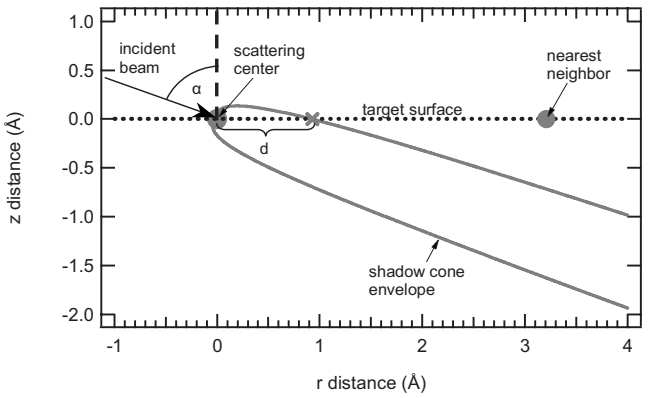

FIG. 2. Shadow cone schematic showing the relationship between the beam angle of incidence, α, and the intersection distance along the target surface, d. The solid line indicates the shadow cone envelope, whereas the dotted line indicates the surface.

tance on the surface, d. (See Fig. 2 for the appropriate geometry.) Agostino *et al.*[5] used this relationship to create real-space scattering maps which indicate local surface structure. Their approach involves obtaining a scattering data set for a wide range of azimuthal (φ) and polar angles (α) at good angular and energy resolution. Agostino *et al.*[5] produced scattering maps of surface atoms on Cu, Al, and Pt single crystals and noted parabolic regions of high scattering intensity, created by shadow cone intersections with surface atoms. The apex of each of these regions appeared to correspond to the location of a neighboring atom on the surface. If this interpretation is correct, scattering maps provide a means to extract local structural information from LEIS data in a straightforward manner. While scattering maps are described in terms of shadow cones, it is important to note that they fully contain all of the scattering data over the range of angles considered. In fact, the scattering intensity patterns in the maps often contain many subtle details owing to contributions from complex scattering events (such as multiple weak sequential collisions). The formalism of relating shadow cone surface intersections with distances is used as an expedient way to render the maps in real space.

Surprisingly, very little subsequent work was performed in this area after the original study of Agostino *et al.*[5] A possible reason is that the process of acquiring the data needed to construct the maps is rather demanding. With the current availability of highly automated instrumentation and increased computing power, generating scattering maps has become much more practicable. Recently, a number of very detailed scattering maps have been published by Rabalais and co-workers.[6,7] It is important to note that these maps were constructed by collecting scattering intensities over a hemispherical region above the sample by varying the detector angle (rather than incidence angle), making them fundamentally different from the maps developed by Agostino *et al.*[5] The ability to render the maps in real space also distinguishes the work of Agostino *et al.*[5] from others.

For this study, we modified the binary collision code MARLOWE (motivated by prior work described in Refs. 8 and 9) and applied it to the model system $Ne^+ \rightarrow Mg(0001)$. Using reliability factors (R factors), these results were then compared with experimental measurements under the same conditions to demonstrate a general method for determining surface-atom positions. Such quantitative comparison techniques have not found widespread use in LEIS studies. The method described here could be extended to compound materials, since LEIS can identify atomic species. Direct recoil spectroscopy (DRS), in which recoiling particles rather than scattered ions are detected, could also be implemented in this manner to detect adsorbed species such as hydrogen. A necessary first step in the process is to apply the scattering map techniques described above to the substrate surface, which is the focus of this paper.

II. EXPERIMENTAL CONFIGURATION

The experimental data were obtained with an angle-resolved ion energy spectrometer (ARIES) system. This instrument has been described in detail;[10] we only provide a brief discussion here. The samples were maintained in a UHV chamber capable of achieving a base pressure of 3×10^{-10} torr. A mass-analyzed source bombarded the samples with low-energy monoenergetic ions in the range of 500 eV–3 keV. A computer controlled five-axis positioning stage allows for a wide range of crystal orientations with respect to the beam, including full 360° rotations in the azimuthal (φ) direction and polar angle settings from 0° to 90°. An electrostatic energy analyzer may be placed at observation angles in the range $15° \leq \theta \leq 90°$. The sample holder was installed through a load lock and included a small heating element for annealing.

The beam itself was rastered over a 2 mm square pattern on the surface. To maintain the same pattern size on the sample with varying incidence angle α, the raster was adjusted accordingly. Typical beam currents were approximately 100–200 nA. The single-crystal Mg(0001) sample was sputter cleaned and annealed to 125 °C prior to exposure to the ion beam. All measurements described in this paper were made at ambient temperature.

III. MARLOWE SIMULATIONS

Numerous computational techniques exist for simulating the interaction of energetic ions with surfaces, most of which can be roughly categorized as either binary collision or molecular-dynamics models.[11] Binary collision codes are computationally efficient and model the substrate with sufficient detail for LEIS simulations. The scattered and recoil energies of interest for LEIS are typically well above 100 eV, an energy range where the binary collision approximation can safely be considered valid.[11,12] With this in mind and due to its ability to model scattering from crystalline targets, MARLOWE (Refs. 12 and 13) was chosen to model our experiments.

A set of user-defined subroutines were added to MARLOWE to tailor the output for LEIS simulations. The primary function of these subroutines was to track particle energies, trajectories, and collision partners, and to output these results in a concise format for analysis. Our modifications to MARLOWE did not affect the evaluation of the scattering in-

tegrals or particle trajectories in the original program but instead identified and retained only trajectories which contributed to the maps. Specialized information such as collision partner identities was also retained. While we found MARLOWE to be quite effective, several other binary collision programs such as SARIC (Ref. 6) or FAN (Ref. 3) could also be programmed to generate the maps in this manner.

The simulation geometry was designed to mimic that of the ARIES instrument as closely as possible. All scattered or recoiled particles escaping from the surface within the same acceptance angle as ARIES were tracked by the program. To ensure that all possible impact conditions were considered, the initial locations of the incident ions were randomly dispersed over a region equivalent to the projected area of a single substrate unit cell. Hence, for the Mg(0001) surface the impact region was a parallelogram. The initial positions of all the incident ions were located one lattice spacing above the surface, ensuring that the primary particles would be initialized at a position well away from the influence of any target atoms.

We modeled the interaction between the incident ion and the target atoms using the Ziegler-Biersak-Littmark[14] (ZBL) interaction potential. In each of the simulations presented in this paper, the target lattice was assumed to be at room temperature. No reconstruction was expected at 300 K for Mg(0001) and only a bulk-terminated surface was considered. Random lattice vibrations are taken into account by introducing a Debye temperature for each lattice site (for magnesium θ_D=400 K).[11] For the first atomic layer, a lower surface Debye temperature θ_D=260 K was assumed.[15] We also incorporated a small 1.9% expansion between the first and second atomic layers into the model.[15]

A common concern with LEIS data is the effect of neutralization which may distort structural information about the surface. While many researchers have addressed this problem, no clear consensus has emerged on handling this issue. We have used a straightforward effective model described by Beikler and Taglauer.[9] With the idea that each collision provides an opportunity for a scattered ion to acquire an electron, a constant survival probability $0 \leq p \leq 1$ is assigned for all such events. Therefore, if a particle undergoes N collisions, its contribution to the ion energy spectrum is weighted by p^N. Following the approach of Beikler and Taglauer,[9] we have assumed that a collision must result in a deflection of at least 4° in order to contribute to neutralization. For 2 keV $Ne^+ \rightarrow Mg(0001)$, we have found through comparison of simulations with experimental data that a survival probability of $0.8 \leq p \leq 0.95$ is appropriate.

The number of incident trajectories to be simulated is dictated by the need for sufficient peak height in the LEIS energy spectrum when compared to the background noise level, and 2×10^6 individual trajectory simulations generally provided satisfactory results. With this number of simulations, identical input files initialized with different random number seeds would yield single-scattering intensities which agreed to within 5%. In addition, for LEIS simulations the trajectories of the primary particles are of the most interest, and significant savings in computational resources were attained by ignoring recoil trajectories. The contribution of direct recoil Mg particles could be avoided by using an ion scattering system configured to detect backscattered particles. However, a forward-scattering configuration was used in the present study because of the ultimate goal of extending this work to obtain recoil maps from adsorbed atoms.

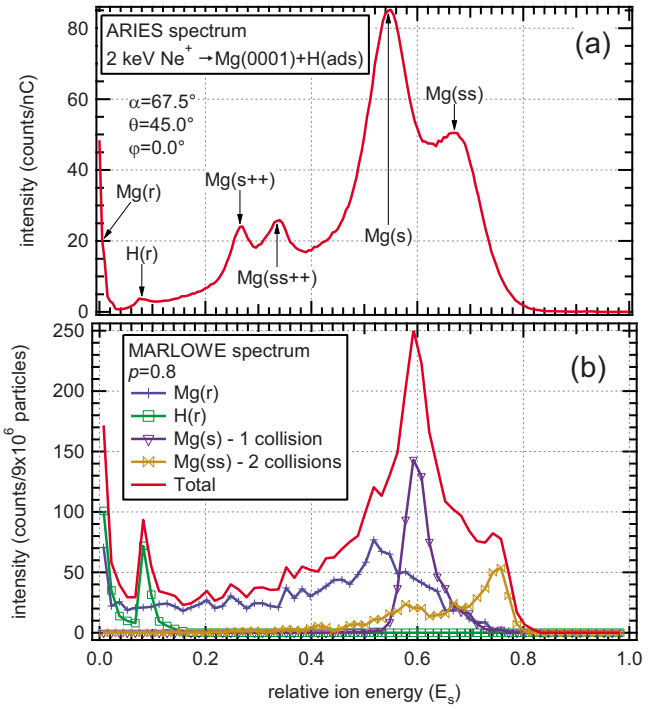

FIG. 3. (Color online) Ion energy spectra for 2 keV $Ne^+ \rightarrow Mg(0001)$ obtained both (a) experimentally and (b) by MARLOWE. In panel (a), the scattering and recoil peaks are indicated for both H and Mg. The spectrum in panel (b) has been decomposed to show contributions from different scattering and recoil processes.

To make the computational work more tractable, no account is made of target damage in the sample. Regardless of any dislocations created by an incident particle, the lattice is reset to its original "pristine" condition for each subsequent ion trajectory. In addition, inelastic losses are not accounted for in collision processes, causing single-scattering peaks in MARLOWE to appear at higher relative energies than those observed experimentally. Furthermore, ionization processes are ignored in this implementation of MARLOWE. These simplifications are not expected to have a major impact on the intensities of the main scattering peaks, which are of primary interest in this work.

IV. COMPARISON OF SELECTED CASES WITH EXPERIMENT

Figure 3(a) displays a LEIS spectrum acquired by the ARIES instrument for 2 keV $Ne^+ \rightarrow Mg(0001)$. The experimental geometry consists of an incidence angle α=67.5°, azimuth angle φ=0°, and scattering angle θ=45°. In this figure, the scattering intensity is plotted as a function of E_s, which is defined as the energy of the scattered ion normalized by the incident energy (E/E_o). The peaks are identified by the substrate atom involved in the collision. Scattering and recoil peaks are given by the notation (s) and (r), respec-

tively. The notation (ss) indicates a double-scattering peak. In addition, portions of the spectrum specifically associated with doubly ionized particles are indicated by the notation ++. Four prominent Mg scattering peaks in the spectrum are identified, along with a low-energy tail associated with Mg(r) and a small H(r) signal from residual hydrogen on the surface. A corresponding MARLOWE plot for the same geometry is shown in Fig. 3(b) for comparison. Note that for this particular case only, a full simulation was conducted, including contributions from recoils. Hence, the simulated data shown in Fig. 3(b) also contain H(r) and Mg(r) components (assuming a recoil survival probability of $p=1$). In general, the H(r) was visible only initially after the sample was exposed to the beam, indicating that most of the measurements described here were obtained for a H-free surface. Also, it is important to note the higher-energy Mg(r) structure which sits below the Mg(s) peak results from multiple collisions and is especially susceptible to neutralization processes. As a result, the Mg(r) signal intensity is greatly overestimated in this region of the spectrum since $p<1$. This provides the justification for ignoring the Mg(r) contribution for the simulations presented in this study, given that the intensity of the Mg(s) peak is of primary interest here. This also eliminates the difficulties associated with estimating separate values of p for the scattered particles and recoils, especially since it is unlikely that the straightforward model described in Ref. 9 would be valid for calculating recoil ion formation rates.

Qualitatively, the simulated and experimental spectra compare well with each other. The elastic Mg(s) and H(r) peaks for the geometry described above are expected to occur at relative energies of 0.577 and 0.09, respectively. Note that the Mg(s) peak measured by the experiment is shifted to slightly lower energies due to inelastic energy losses not accounted for by the MARLOWE simulation. In addition, peaks corresponding to multiply ionized (Ne^{++}) are also absent from the simulated spectrum. In the MARLOWE simulation, 10% of the adsorption sites were randomly populated with H, so that the simulated H(r) signal intensity is comparable to the experimental value. MARLOWE allows the ion energy spectrum to be decomposed in order to distinguish contributions from different scattering and recoil processes. In Fig. 3(b), individual spectra from Mg and H recoils as well as single and double scattered Ne^{+} ions are displayed. Each component contributes a distinct peak to the composite spectrum.

An azimuthal scan showing the variation in the Mg(s) peak intensity over the entire 2π range was acquired by the ARIES instrument and appears in Fig. 4(a). For this case, the incidence and scattering angles correspond to $\alpha=80°$ and $\theta=55°$, respectively. At this incidence angle, the shadow cone edge from a scattering center will intersect the fourth nearest neighbor on the surface. As can be seen from the ARIES plot, increased Mg(s) intensity at angles $\pm 19.1°$ away from the close-packed directions corresponds to enhanced scattering from these neighboring atoms. A MARLOWE plot generated from $\varphi=0°$ to 120° with the same geometry reproduces this behavior precisely. To cover the entire 2π range, the MARLOWE data have been reflected every 120°.

In Fig. 5(a), polar scans showing the variation in the Mg(s) intensity as a function of α along the directions [010], $[\bar{1}20]$, and $[\bar{1}10]$ are shown. With respect to the nearest close-packed direction, these azimuths correspond to $\varphi=0°$, 19.1°, and 30°, respectively. To emphasize the relative shapes of each curve, the intensities have been normalized to their peak values. At grazing incidence ($\alpha>70°$), each of these polar scans is characterized by a strong peak, followed by a rapid decrease in intensity. These peaks may be interpreted by considering the shadow cone geometry for 2 keV $Ne^{+}\rightarrow Mg$. As illustrated in Fig. 1(b), for a given scattering center (labeled as A), a nearest-neighbor atom on the surface (labeled as B) is aligned along the [010] direction. If a ZBL potential is used, the shadow cone edge from scattering center A interacts with atom B at an incidence angle of $\alpha=72°$. A peak in the scattering intensity is visible at this angle in the ARIES spectrum due to the focusing effect near the shadow cone boundary. The situation is more complex along the $[\bar{1}20]$ azimuth, where we observe a maximum in the Mg(s) signal at $\alpha=80°$. This corresponds to the intersection of the shadow cone from the scattering center with the fourth nearest-neighbor atom on the surface (indicated by atom D), although weak interactions with other neighboring atoms also contribute to the scattering intensity at this location. Note that this polar angle corresponds to the value used in the azimuthal scans in Fig. 4.

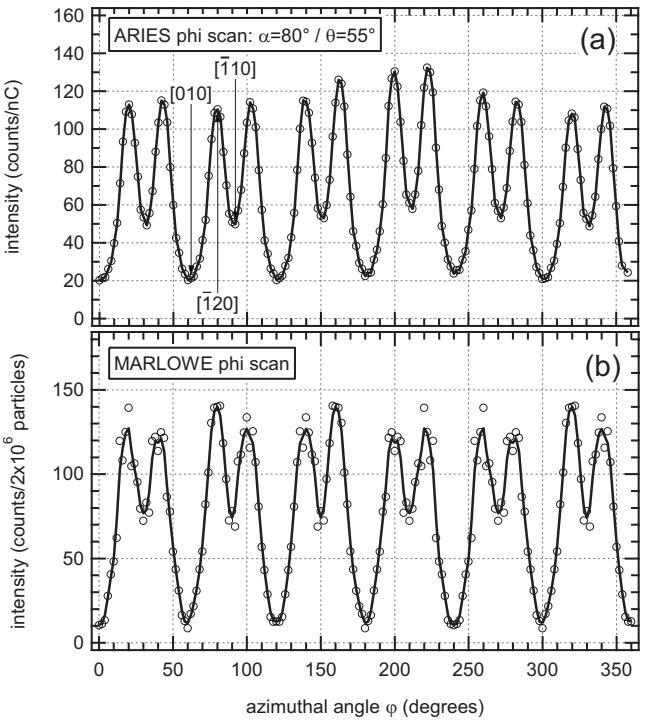

FIG. 4. Scan showing the variation in the Mg(s) peak as a function of azimuthal angle φ. Case (a) was obtained with the ARIES instrument and case (b) was simulated with MARLOWE. The intensity maxima occur 19° away from the close-packed direction and correspond to scattering from the fourth nearest-neighbor atoms on the surface. To account for all possible symmetry planes, the MARLOWE data have been reflected every 120°.

The behavior observed above with the experiment is reproduced well by the MARLOWE simulations shown in Fig. 5(b). Here, we used a neutralization probability of $p=0.9$ for

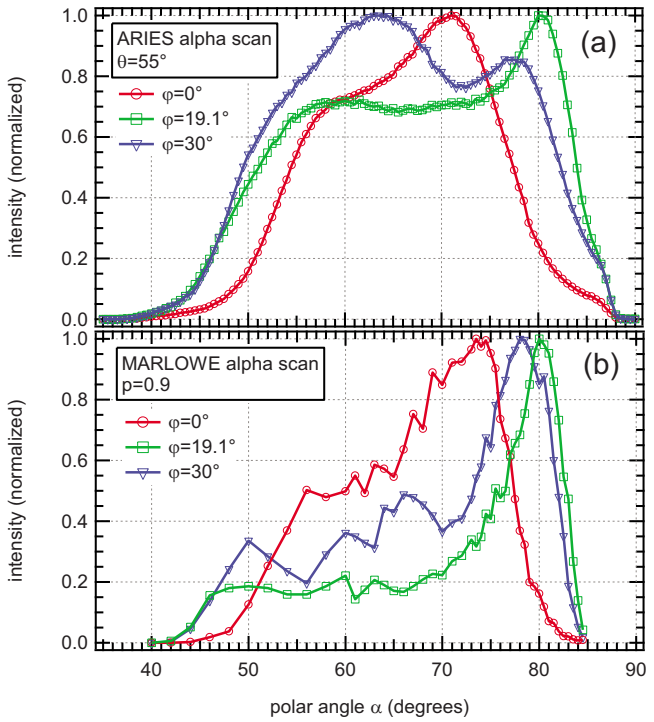

FIG. 5. (Color online) Polar scans along selected azimuths, obtained both (a) experimentally and (b) by simulation.

this analysis. The locations of the grazing incidence peaks in Mg(s) intensity agree with the experiment and with the values calculated from the shadow cone shape. The relative intensity of the peaks at lower angles of incidence is not reproduced as satisfactorily by the simulations. These features correspond to distances smaller than 3 Å from the scattering center and involve subsurface scattering events rather than shadowing of atoms in the surface plane.

V. ION SCATTERING MAPS

Using MARLOWE, we generated ion energy spectra for 2 keV $Ne^+ \rightarrow Mg(0001)$ using a full range of beam incidence angles, α, and sample azimuths, φ. Experimental measurements were taken for the same conditions using the ARIES experiment. The beam incidence angles were selected so as to give a constant increment in the shadow cone intersection with the surface of 0.25 Å in radial distance from the scattering centers over the range from 1.25 to 10.0 Å. The intersection points d were determined using the methods outlined by Hird[16] to model the shadow cone shape. At each incidence angle, ion energy spectra were recorded as the sample azimuth was varied in 2° steps.

For the experimental measurements, a full data set over a complete 360° rotation of the sample consisted of 6480 individual spectra. Each spectrum measured the intensity of detected ions at a relative energy, E_s, from 0 to 1 in 0.005 energy steps with a dwell of 0.025 μC/step. A total dose of 33 mC was required to obtain a full data set. As the ion beam was rastered over a 2×2 mm^2 region, this corresponds to a total fluence of 5×10^{18} Ne/cm^2. Although the surface was being continuously eroded during the measurement, the LEIS data indicated that it remained well ordered. No degradation in the intensity patterns was observed with increasing ion fluence. The MARLOWE maps were generated from 37 azimuthal scans, with φ varying in each case over a range of $0° \leq \varphi \leq 120°$ to account for all possible symmetry planes. (Hence, the MARLOWE results are reflected every 120°.) At each location in the map, a complete ion energy spectrum was generated from 2×10^6 incident ions with bin width of $\Delta E_s = 0.02$.

Surface maps obtained with the ARIES instrument and MARLOWE are presented in Fig. 6 for a detector angle of $\theta = 45°$. A scattered energy of $E_s = 0.6$, which corresponds to single-scattered Ne^+ from the Mg surface, is shown, with the plot coloration indicating scattering intensity. In general, the simulation shows satisfactory agreement with the experimental work. At distances of 3–5 Å from the scattering center, we observed parabolic regions of increased scattering intensity similar to those noted by Agostino *et al.* in Ref. 5.

Figures 6(c) and 6(d) show ARIES and MARLOWE maps for multiply scattered Ne^+ at an energy of $E_s = 0.69$. As before, we have used a detector angle of $\theta = 45°$. The simulated results agree well with the experimental map, with both showing regions of high intensity in the vicinity of the nearest-neighbor atoms. A sixfold symmetry is observed in the experimental case. In a MARLOWE simulation of scattering from a perfect bcc crystal, only one of two possible atom locations in the second layer is occupied and the simulated map has threefold symmetry. The crystal surface used in the experiment, on the other hand, contains step edges which expose both possible configurations. To account for this, the simulated data have been reflected every 120° and averaged together.

Note that scans along a constant α or φ may be interpreted as radial or azimuthal "cuts" in the real-space scattering maps, respectively. For example, a φ scan with $\alpha = 80°$ would correspond to the dashed circle in Fig. 6(b). Polar scans along the [010], [$\bar{1}$20], and [$\bar{1}$10] azimuths are shown by the dashed lines in the Fig. 6(b) overlay. The data shown in Figs. 5 and 6 were acquired for the same values of α and φ, although with a different θ. (Since the cross section for scattering is smaller for larger θ, the overall scattering intensity would be affected. However, the structural information would not be altered.)

The intensity patterns seen in the map are the result of shadow cone edges intersecting neighboring atoms. Many scattered particle trajectories converge at shadow cone edges and locally enhance the flux, which leads to an increase in signal intensity when a cone edge passes through a neighboring atom. To see how the observed structures arise, consider Fig. 7, which shows the elliptical intersections of a shadow cone with the surface plane for several projectile incidence angles α. In this figure, the positions of two neighboring atoms are indicated and the incident-particle direction is initially along the interatomic axis. At incidence angle (a), the edge of the shadow cone formed by the first atom intersects the second atom at a single point. At larger (i.e., more glancing) incidence angles (b, c, d, and e), the second atom lies inside the shadow cone. However, as shown for c, an azimuthal rotation by an angle $\Delta\varphi$ will bring the second atom onto the edge of the shadow cone.

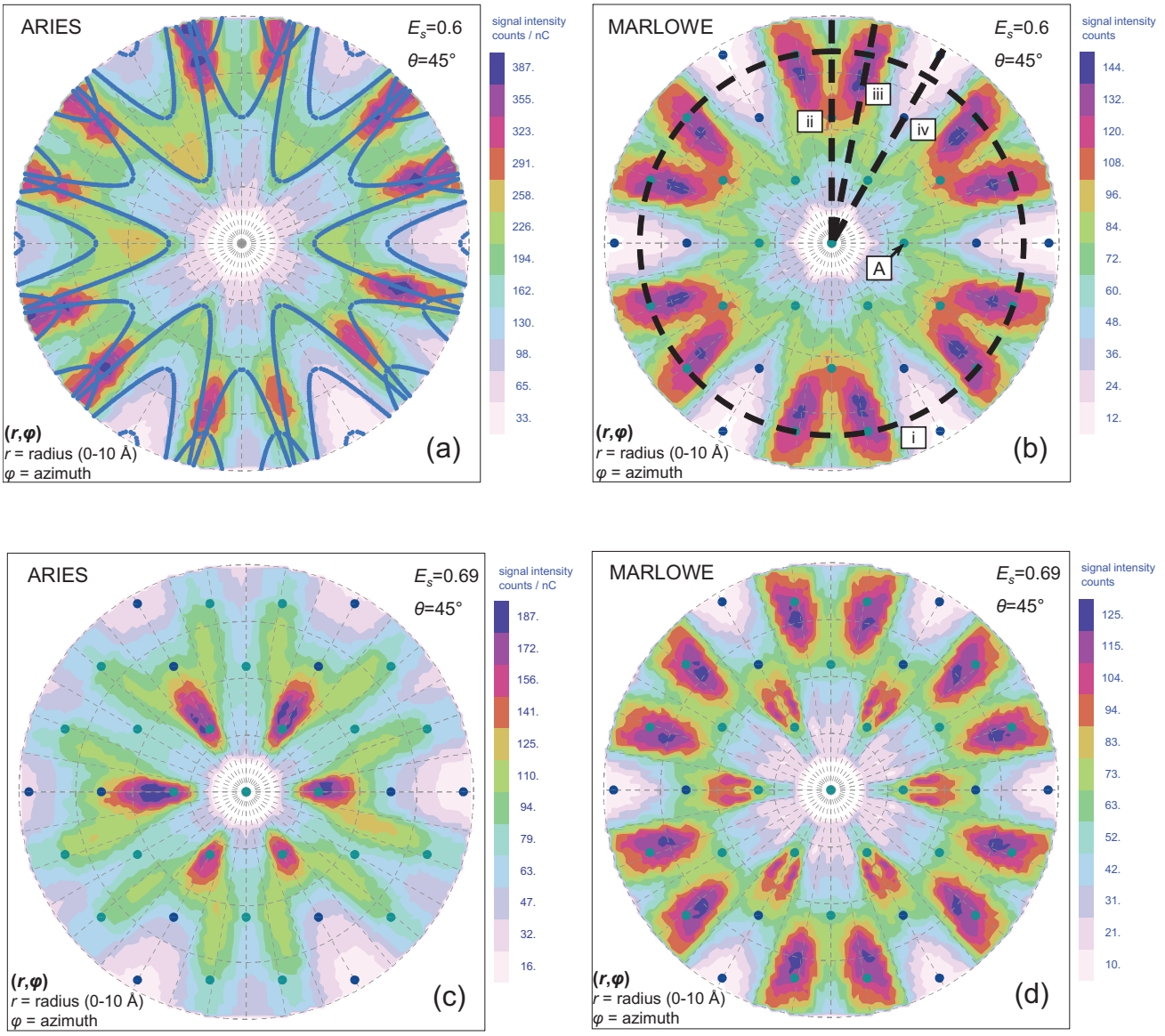

FIG. 6. (Color) Real-space scattering maps of the Mg(0001) surface using LEIS generated by analyzing scattered 2 keV Ne^+ ions at a scattering angle of θ=45°. ARIES and MARLOWE maps are shown for both the single-scattered [in panels (a) and (b)] and doubly scattered [in panels (c) and (d)] ions. The overlay in panel (a) depicts the calculated shadow lines.

Associating the incidence angle with radial distance, as was done to construct the map, we thus expect a signal enhancement at the location of the atom at incidence angle (a) and at locations beyond the atom and offset by the appropriate $\Delta\varphi$ for larger incidence angles. The resulting shadow cone intersection line on the surface can be simply parametrized in the form $y=b_1\sqrt{x}+b_2x$. For the case of 2 keV Ne^+ scattering from Mg, the constants are $b_1=0.540$ and $b_2=0.221$. This function is plotted in Fig. 6(a) overlay for the first through fifth atom neighbors on Mg(0001). The intensity patterns observed in the experimental Mg(s) map to a large extent correspond with the shape of these lines. Further, regions of the highest signal intensity occur at atom positions where shadow cone intersection lines overlap. The highest scattered particle flux is focused at these locations.

For the purpose of identifying atom locations based on a scattering map of an unknown surface, one could first envision referring to an ion energy spectrum to characterize the surface composition. This would also reveal which scattering processes are depicted in the map. Any symmetry of the surface structure should be immediately evident, and the approximate nearest-neighbor atom locations can be assigned to the apices of the parabolic structures nearest to the reference site. A fitting algorithm could potentially be developed to correlate the exact atom positions to the parabolic intensity patterns in the maps. However, focusing effects can affect the parabolic intensity structures. Using the *R*-factor analysis described in Sec. VI of this paper to compare simulated configurations with the experimental data is an alternate approach.

One potential disadvantage of the scattering maps is the large primary ion dose needed to obtain them, which causes surface damage. However, several strategies can be implemented to mitigate this problem. For example, one could

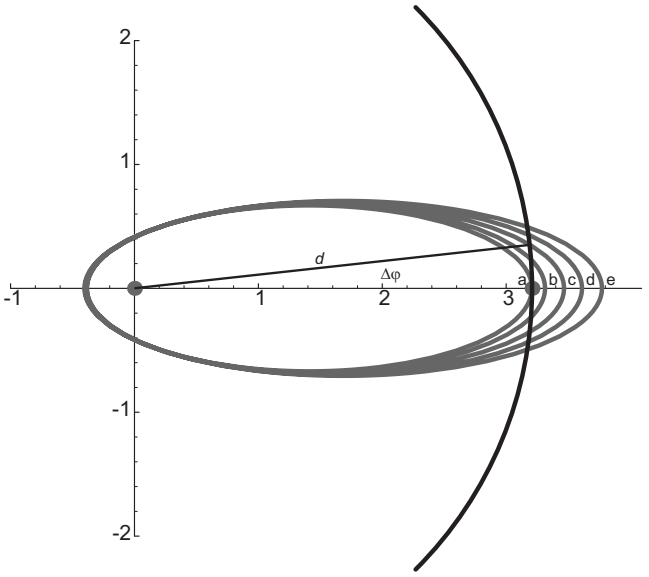

FIG. 7. Schematic depicting the intersection curves between the shadow cones and the surface plane.

take advantage of symmetry and not acquire scattering intensity over a full 360° azimuthal range. Also, rather than acquiring a full spectrum for each map point, one could take measurements only at specific energies of interest, thereby reducing the needed dose by at least a factor of 10. As an alternative, the added sensitivity that a time-of-flight detector provides could further reduce the required dose by several orders of magnitude.

VI. ANALYSIS OF SURFACE STRUCTURE

The agreement between the MARLOWE and ARIES maps appears satisfactory from a qualitative standpoint. Because the intensity patterns correspond directly to atom locations on the surface, any major difference between the simulated and experimental configurations should be obvious. However, it is worth considering whether more detailed information (such as lateral interatomic spacing on the surface) could be measured. This is an area where comparisons between experiments and simulations would be particularly helpful, especially if a quantitative comparison between a series of subtly different configurations was possible. While it is unlikely that LEIS would be able to improve on existing methods for determining lattice constants, improved characterization of adsorbate locations may be feasible with DRS. Although LEIS could also be used to determine the spacing between atomic layers, the present discussion will be restricted to determining positions within the surface plane.

A common practice in surface structure studies using low-energy electron diffraction is to use reliability factors (R factors) as a means of comparison between theoretical results and experiments.[17] To date, it appears that this method has not been extensively adopted in LEIS studies. The ion scattering maps presented here provide the possibility of comparing large sets of data, allowing one to fit the entire map with the model rather than a small set of scattering peaks. This has the additional benefit of reducing the impact of any localized errors.

A key point which should be considered when comparing LEIS experiments with simulations is that the locations of the scattering peaks and the subsequent rapid decrease in intensity as an adjacent atom moves into a shadow cone contain the most information about the structure of the surface. The relative intensities of closely spaced peaks are of lesser importance, and absolute intensities are not relevant for this purpose. Hence, any method of comparison should emphasize peak positions along with the "critical edge" location and remove any dependence on absolute intensity. To accomplish this task, we used a weighted least-squares method to scale the simulated data and achieve the best possible match with the experiment. This mathematical technique has been used in a variety of other applications, including the analysis of gamma-ray spectra.[18] The individual points from the experimental (y) and simulated (a) data sets are related by

$$y_i = ma_i + \varepsilon_i.$$

In the above equation, ε_i is the error between the two data sets at location i when the scaling factor m is applied. Note that for two slightly misaligned peaks, the error term becomes very large at the peak edges.[18] This provides a high level of sensitivity to the critical edge phenomena mentioned above. To emphasize the peak locations, we define a weight factor matrix $\boldsymbol{W}$, with the diagonal elements W_{ii} assigned values which are proportional to the number of counts at each position i. The scaling factor $\hat{m}$ which minimizes the error term is then

$$\hat{m} = (\mathbf{a}^{\mathbf{T}}\mathbf{W}\mathbf{a})^{-1}\mathbf{a}^{\mathbf{T}}\mathbf{W}\mathbf{y}.$$

Note that $\mathbf{a}$ and $\mathbf{y}$ are vectors containing the simulated and experimental data sets, respectively. Applying this scaling to the simulated spectrum, one may then proceed to calculate an R factor. There are numerous possible definitions,[17,19] although we have found the following version to be effective:

$$R = \frac{1}{N}\sum_{i=1}^{N}\frac{(y_i - \hat{m}a_i)^2}{[y_i^2 + (\hat{m}a_i)^2]}.$$

Note that N corresponds to the total number of map locations included in the comparison. To compile the simulated data set, MARLOWE calculations were performed along specific azimuths in the scattering maps, as shown in Fig. 8. The lateral lattice spacing was varied over a range of values between $\pm 10\%$ of the nominal case ($a_o = 3.2094$ Å).

To validate the method described above, we first compared different configurations along individual azimuths with the nominal simulated case as the reference condition. The R-factor variation for three representative azimuths is shown in Fig. 9(a). The result is less than satisfying however, as one would expect each of these curves to trend toward higher values as the deviation in a_o from the reference value increases. The variation in the R factor is somewhat erratic over the range of a_o considered here, making the comparisons difficult to interpret. The comparison clearly benefits from increasing the size of the data set considered. Consider

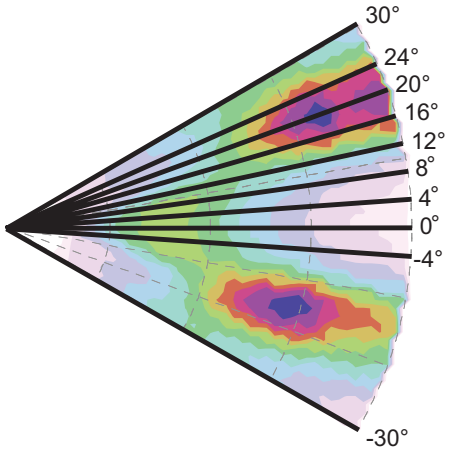

FIG. 8. (Color) Sector of the Mg(s) ion scattering map showing azimuths which were included in the comparison between the full ARIES and MARLOWE maps.

the "full map" comparison shown in Fig. 9(b). Note that in this case, each simulated configuration includes a set of ten azimuths. A single value of $\hat{m}$ is fitted for the entire data set, allowing the areas of highest scattering intensity to be emphasized. The variation in the R factor is well behaved and smoothly approaches a minimum as the deviation from the reference (nominal) case decreases.

The final step is to compare between the experimental ARIES data and the simulated MARLOWE configurations. The results are shown in Fig. 9(c). For this analysis, the simulated data sets included polar scans along ten azimuths, as described previously for MARLOWE full map comparison. These comparisons were repeated at 60° azimuthal intervals to exploit symmetries evident in the maps. Three different values of the neutralization probability are also considered. Note that the R factors for these comparisons reach a minimum value for a lattice constant of $a_o \approx 3.1$ Å, approximately 0.1 Å lower than the nominal value. Furthermore, the agreement between the simulation and the model appears to improve with a higher value of p, supporting our previous assertion that neutralization is rather slight for experimental conditions examined here.

A basic question is to what accuracy can interatomic distances be measured experimentally? This depends partially on how precisely the target crystal surface can be oriented with respect to the ion beam, since the distance along the surface is determined from α. For the case described above, a $\pm 10\%$ change in lattice spacing causes the scattering intensity pattern to shift by approximately $\pm 1°$ in α. This is well within the resolution of our ARIES system, as the alignment procedure for the sample positioning stage with the ion beam allows α to be calibrated to within $\pm 0.1°$. Given the shadow cone shape, the error in distance d from any sample misalignment would be more severe for large α. However, even at $\alpha = 80.5°$, which corresponds to the outer edges of the ion scattering maps ($d = 10$ Å), the error in calculated distance would be ± 0.15 Å for a misalignment in α of $\pm 0.1°$. The 0.1 Å difference between the value of a_o predicted by the comparison between the simulation and the experiment is certainly within this range. It is also important to note that while the ZBL potential has been empirically fitted to a large number of potentials, there is likely to be some degree of error when it is applied to a specific system. For a known surface, one could remove the error mentioned above using a Moliére potential[14] and calibrating the screening length to give the accurate lattice parameter. This process is demonstrated in Fig. 10 using R-factor analysis, where the simulated polar scans along the high-symmetry azimuths ($\varphi = 0°$, 19.1°, and 30°) are compared with ARIES data along the same directions. In each case, the screening length was altered by a multiplicative constant, with values in the range of 0.75–0.80, providing the best fit to the ARIES data. We envision that once the complete map is used to fit the screening length, the same procedure as was used with the ZBL potential could be implemented to determine the atom spacing.

VII. CONCLUDING REMARKS

In this study, we have developed a technique that uses experimental and simulated low-energy ion scattering maps

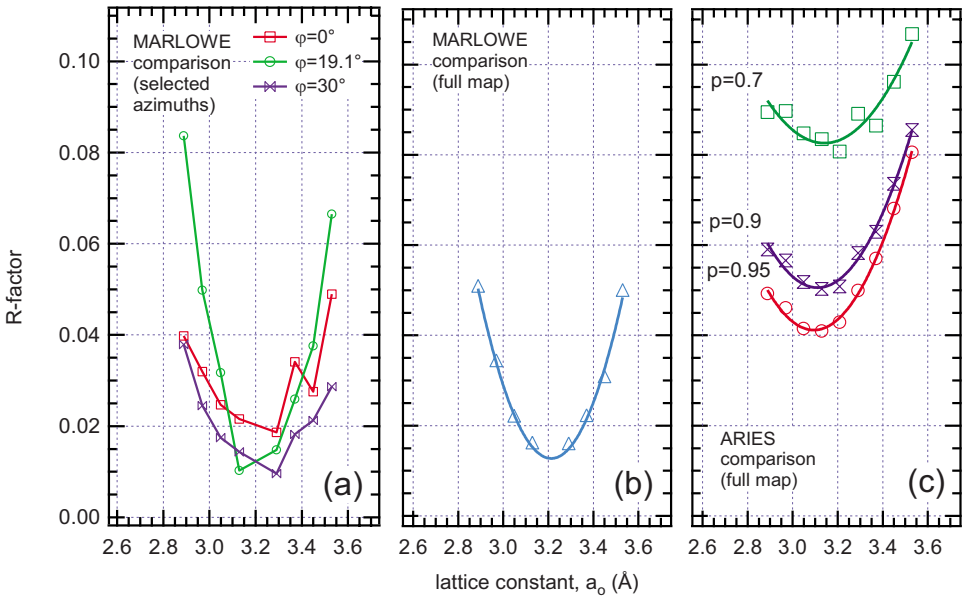

FIG. 9. (Color online) R-factor variation as a function of lateral lattice spacing. The reference condition corresponds to the nominal Mg spacing ($a_o = 3.2094$ Å). (a) MARLOWE-MARLOWE comparison for individual azimuths. (b) MARLOWE-MARLOWE comparison over the full map. (c) ARIES-MARLOWE comparison over the full map, showing the impact of different ion survival probabilities (p).

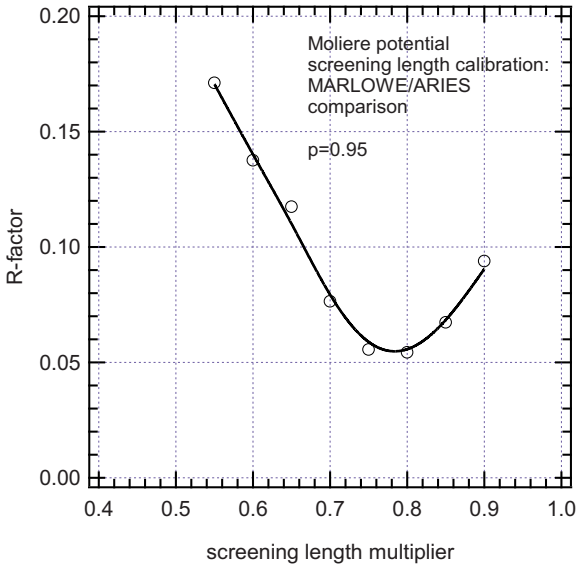

FIG. 10. (Color online) Calibration of the Moliére potential screening length using *R*-factor analysis. Polar scans along the high-symmetry azimuths (φ=0°, 19.1°, and 30°) were used as the basis for the comparison, and the screening length was varied by a multiplicative factor.

to characterize surface structure. This is a significant improvement over previously used methods of extracting such information that involve monitoring scattering intensity along constant azimuths (φ) or at constant angles of incidence (α). In much of the prior work in this area, computer simulations of LEIS have similarly been restricted to a narrow set of scattering conditions.

A real-space scattering map generated for a complete set of azimuths and polar angles enables surface structure to be determined in a straightforward manner. Scattering maps for $Ne^+ \rightarrow Mg(0001)$ were obtained by both the ARIES experiment and MARLOWE simulations. To our knowledge, the simulated maps described in this work represent the first simulation of full ion scattering maps in this manner. Atomic positions can be deduced from the scattering patterns evident on these maps by comparing a simulated configuration to the experimental results using *R* factors.

Given the appropriate circumstances, there do not appear to be any major obstacles to applying the real-space mapping techniques described here to adsorbate layers. An important first step in this analysis is to generate a map of the substrate to serve as a reference for the adsorbate layer. The techniques described in this paper therefore lay the groundwork for further use of scattering maps.

ACKNOWLEDGMENTS

We would like to express our appreciation to Dean Buchenauer for his assistance with the computer modeling. In addition, we thank Norman Bartelt and Kevin McCarty for providing many useful comments. Sandia is a multiprogram laboratory operated by Sandia Corporation, a Lockheed Martin Co., for the National Nuclear Security Administration, United States Department of Energy (Contract No. DE-AC04-94AL85000).

*Mailing address: Sandia National Laboratories, P.O. Box 969, MS 9161, Livermore, CA 94551. rkolasi@sandia.gov

[1] D. P. Smith, Surf. Sci. **25**, 171 (1971).
[2] R. S. Williams and J. A. Yarmoff, Nucl. Instrum. Methods Phys. Res. **218**, 235 (1983).
[3] H. Niehus, W. Heiland, and E. Taglauer, Surf. Sci. Rep. **17**, 213 (1993).
[4] F. Samavat, B. V. King, and D. J. O'Connor, Surf. Rev. Lett. **14**, 31 (2007).
[5] R. G. Agostino, P. Aebi, J. Osterwalder, J. Hayoz, and L. Schlapbach, Surf. Sci. **384**, 36 (1997).
[6] V. Bykov, L. Houssiau, and J. W. Rabalais, J. Phys. Chem. B **104**, 6340 (2000).
[7] C. Höfner and J. W. Rabalais, Phys. Rev. B **58**, 9990 (1998).
[8] H. Derks, A. Närmann, and W. Heiland, Nucl. Instrum. Methods Phys. Res. B **44**, 125 (1989).
[9] R. Beikler and E. Taglauer, Nucl. Instrum. Methods Phys. Res. B **182**, 180 (2001).
[10] R. Bastasz, J. A. Whaley, T. A. Lograsso, and C. J. Jenks, Philos. Mag. **86**, 855 (2006).
[11] W. Eckstein, *Computer Simulation of Ion-Solid Interactions* (Springer-Verlag, Berlin, 1991).
[12] M. T. Robinson and I. M. Torrens, Phys. Rev. B **9**, 5008 (1974).
[13] M. T. Robinson, Phys. Rev. B **40**, 10717 (1989).
[14] J. F. Ziegler, J. P. Biersack, and U. Littmark, *The Stopping and Range of Ions in Solids* (Pergamon, New York, 1985).
[15] P. T. Sprunger, K. Pohl, H. L. Davis, and E. W. Plummer, Surf. Sci. **297**, L48 (1993).
[16] B. Hird, Can. J. Phys. **69**, 70 (1991).
[17] J. B. Pendry, J. Phys. C **13**, 937 (1980).
[18] E. Schonfeld, A. H. Kibbey, and W. Davis, Jr., Nucl. Instrum. Methods **45**, 1 (1966).
[19] Y. Kuk and L. C. Feldman, Phys. Rev. B **30**, 5811 (1984).